ACS APPLIED MATERIALS & INTERFACES

Research Article

www.acsami.org

Yield Point of Semiconducting Polymer Films on Stretchable Substrates Determined by Onset of Buckling

Adam D. Printz, Aliaksandr V. Zaretski, Suchol Savagatrup, Andrew S.-C. Chiang, and Darren J. Lipomi*

Department of NanoEngineering, University of California, San Diego, 9500 Gilman Drive, Mail Code 0448, La Jolla, California 92093-0448, United States

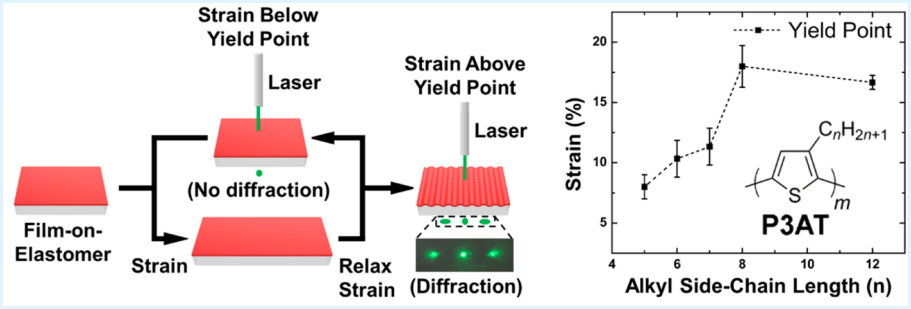

ABSTRACT: Mechanical buckling of thin films on elastomeric substrates is often used to determine the mechanical properties of polymers whose scarcity precludes obtaining a stress−strain curve. Although the modulus and crack-onset strain can readily be obtained by such film-on-elastomer systems, information critical to the development of flexible, stretchable, and mechanically robust electronics (i.e., the range of strains over which the material exhibits elastic behavior) cannot be measured easily. This paper describes a new technique called laser determination of yield point (LADYP), in which a polymer film on an elastic substrate is subjected to cycles of tensile strain that incrementally increase in steps of 1% (i.e., 0% → 1% → 0% → 2% → 0% → 3% → 0%, etc.). The formation of buckles manifests as a diffraction pattern obtained using a laser, and represents the onset of plastic deformation, or the yield point of the polymer. In the series of conjugated polymers poly(3-alkylthiophene), where the alkyl chain is pentyl, hexyl, heptyl, octyl, and dodecyl, the yield point is found to increase with increasing length of the side chain (from approximately 5% to 15% over this range when holding the thickness between ∼200 and 300 nm). A skin-depth effect is observed in which films of <150 nm thickness exhibit substantially greater yield points, up to 40% for poly(3-dodecylthiophene). Along with the tensile modulus obtained by the conventional analysis of the buckling instability, knowledge of the yield point allows one to calculate the modulus of resilience. Combined with knowledge of the crack-onset strain, one can estimate the total energy absorbed by the film (i.e., the modulus of toughness).

KEYWORDS: *yield point, thin films, organic semiconductors, P3ATs, buckling-based metrology, film-on-elastomer system*

1. INTRODUCTION

Thin-film organic conductors and semiconductors are promising materials for the fabrication of robust devices capable of surviving the repetitive strains applied during use in portable, outdoor, and wearable or implantable applications.[1−6] In these applications, permanent (or plastic) deformation is often undesirable, except in the cases in which one-time bonding to nonplanar surfaces is required.[7,8] Ideally, the materials used would remain in the elastic regime, below the yield point, at the strains expected to be reached during normal use. For bulk materials, the yield point can be obtained using a tensile test. However, the scarcity of materials such as conjugated polymers, of which only a few hundred milligrams may be obtained in a laboratory-scale synthesis, precludes obtaining these measurements using a tensile test. To conserve material, performing mechanical testing on thin films is ideal, however, there are difficulties associated with isolating and manipulating free-standing films of submicron thickness. We thus developed a new method based on the onset of buckling of a film on an elastomer, which we call laser determination of yield point (LADYP). LADYP measurements are performed by cyclically straining and relaxing a polymer film on an elastomeric substrate and then recording the strain at which a diffraction pattern appears when irradiated with a laser beam. When the yield point is reached, the thin film plastically deforms, and upon relaxation, the film is compressed and surface wrinkles are formed which then diffract the light.[9,10] Although other buckling-based metrology techniques have compressed unstrained thin films and used laser diffraction (or micrographs) to measure their tensile modulus,[9−12] LADYP is the first technique that compresses plastically deformed films and uses laser diffraction to determine their yield point.

We used this technique to explore the effects of the alkyl side-chain length, as well as the film thickness, on the yield

Received: August 11, 2015
Accepted: October 6, 2015
Published: October 6, 2015

DOI: 10.1021/acsami.5b08628
ACS Appl. Mater. Interfaces 2015, 7, 23257−23264

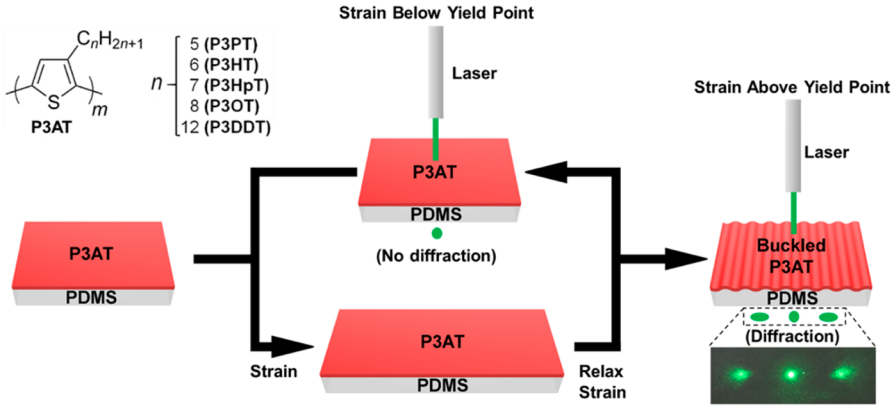

Figure 1. Schematic diagram of the procedure and the molecular structure of the polymers studied in this work. Each polymer thin film was transferred to PDMS and then stretched and relaxed with subsequently increasing strain with each cycle. At the point of relaxation, laser was transmitted through the film, and above the yield point, the film buckled and diffracted the laser. A photograph of the diffraction peaks is included in the inset.

point of poly(3-alkylthiophene)s (P3ATs) (Figure 1), which are excellent model polymers due to their relatively simple molecular structure comprising repeat units of thiophenes with alkyl side chains. We previously measured the tensile modulus, the inverse of mechanical compliance, and ductility of P3ATs, as manifested in their crack-onset strains, and found that these parameters are related to the alkyl side-chain length, with longer side-chains leading to more compliant and ductile films.[11,12] We expected that the yield point would follow a similar trend. In addition to the effect of alkyl side-chain length, we explored the effects of film thickness on the yield point. Others had previously shown that decreasing film thickness depresses the glass transition temperature of thin films,[13−16] and we hypothesized that this would lead to an increase in yield point in P3ATs, as has been shown for polystyrene and poly(2-vinylpyridine) using a relatively complex method.[17,18] Our goal was thus to develop a simple procedure to measure the yield point using similar equipment, an actuator, a laser, and a microscope, to those already used routinely to measure tensile modulus and crack-onset strain.

2. BACKGROUND

Mechanical properties are often assumed to be favorable in all organic conductors and semiconductors, and thus, the selection of materials for a given application is made on the basis of electronic performance.[7,19,20] For example, poly(3-hexylthiophene) (P3HT) is the most prevalent semiconducting polymer in the literature because of its good electronic performance,[21−27] yet it has a high tensile modulus (stiffness) and is brittle at common laboratory temperatures.[11,28] Although the modulus is a critical parameter when designing a flexible or stretchable system with reduced interfacial stresses, it does not, however, predict the range over which a thin film exhibits elastic behavior. Most conjugated polymers crack in the regime of plastic deformation; it is therefore important to determine the yield point. For thin films, measurement of the yield point has not been straightforward[29,30] because of the difficulty of isolating and manipulating films with submicrometer thicknesses.[9,11,31−34] Kim and co-workers have developed specialized equipment to perform stress−strain measurements of films supported by liquid, but this is a potentially limited method due to the requirements that the liquid have high surface tension and low viscosity and that the thin film must be compatible with the liquid, though under favorable circumstances this technique can generate the entire stress-strain curve.[35,36]

Given the difficulty of manipulating free-standing films, mechanical properties are often determined indirectly using film-on-elastomer (FOE) systems. The most well-known method is the buckling-based metrology originally developed by Stafford and co-workers,[9,11,37] which exploits the buckling instability (surface wrinkling) that occurs when a relatively rigid film is compressed on a relatively soft elastomeric substrate (such as PDMS which, because of its high elasticity when not treated with oxygen plasma or UV-ozone, will not contribute buckles of its own under small compressive strains). The buckling wavelength is related to the balance between the energy required to bend the rigid substrate and that required to deform the soft substrate and can be used to calculate the tensile modulus of the thin film.[10] The strain to fracture is generally measured indirectly by recording the strain at which the first crack appears in a film on a stretchable substrate.[38,39] However, the crack-onset strain is indirectly connected to ductility because it is also a function of adhesion of the film to the substrate: films that are well adhered to their substrates have high crack-onset strains.[11,40] To date, only the tensile modulus and crack-onset strain can be extracted easily from FOE systems, whereas previous methods for measuring the yield point are substantially more complex and limited to certain types of polymers.[17,18] Other properties relevant to mechanical reliability in flexible devices, such as adhesion and cohesive fracture energy, can also be obtained from thin films in other configurations.[29,30]

Figure 2 illustrates the information easily obtainable from FOE systems superimposed on a hypothetical stress−strain curve obtained from a conventional pull tester. Although the tensile modulus obtained from the buckling-based metrology defines the initial slope of the curve, and the crack-onset strain defines its end point, the width of the elastic regime is not defined, and thus the range over which the polymer could be deformed without plastic deformation is not known. Moreover, without defining the upper limit of strain at the yield point, the energies absorbed by the polymer in the elastic regime (i.e., the resilience) and the total energy absorbed at the point of fracture (i.e., the toughness) cannot be known. Knowledge of the yield point "calibrates" the curve: it permits calculation of the resilience and a rough estimate of the toughness. Beyond

DOI: 10.1021/acsami.5b08628
ACS Appl. Mater. Interfaces 2015, 7, 23257−23264

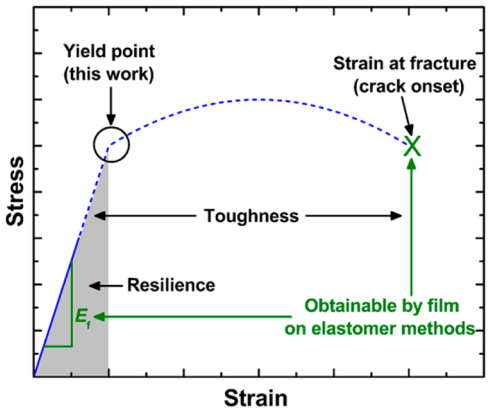

Figure 2. Hypothetical stress–strain curve for a bulk polymer. The elements in green, the tensile modulus and the strain at fracture, have been previously measured by film-on-elastomer systems. Measurement of the yield point is reported in this work. The area between the yield point and the strain at fracture is the plastic regime, which is still not measurable for thin films on elastomeric substrates.

knowledge of the resilience and toughness, it is technologically relevant to define the amount of strain a thin film can undergo before plastically deforming. The required accommodation of strain can vary greatly depending on the intended use of a device, and understanding the material limits (e.g., elasticity) is necessary in the selection of appropriate materials for specific applications. For example, a device worn to measure a pulse will undergo much less strain (<1%) than a device worn on an elbow when it bends (>50%).[41] Although a material that might have higher electronic performance, but a low yield point, would be appropriate for the former application, a sacrifice of electronic performance might be required to ensure that the device can maintain predictable performance at high strains in the latter application.

3. EXPERIMENTAL METHODS

3.1. Materials. Poly(3-pentylthiophene) (P3PT, M_n = 13 kDa, PDI = 2.5), poly(3-heptylthiophene) (P3HpT, M_n = 35 kDa, PDI = 1.5), and poly(3-dodecylthiophene) (P3DDT, M_n = 21 kDa, PDI = 1.8) were purchased from Rieke Metals, Inc. and used as received. Poly(3-hexylthiophene) (P3HT, M_n = 44 kDa, PDI = 2.0) and poly(3-octylthiophene) (P3OT, M_n = 34 kDa, PDI = 2.5) were purchased from Sigma-Aldrich and used as received. (Although the authors note this is a large range of M_n, a previous study by us showed that the difference in tensile modulus between P3HT with M_n = 6.25 kDa, PDI = 1.2 and M_n = 14.5 kDa, PDI = 2.0 was negligible.)[42] PDMS, Sylgard 184 (Dow Corning), was prepared according to the manufacturer's instructions at a ratio of 10:1 (base:cross-linker) and cured at 75 °C for 25 min before it was used for mechanical testing. (Tridecafluoro-1,1,2,2-tetrahydrooctyl)-1-trichlorosilane (FOTS) was obtained from Gelest. Chloroform, acetone, and isopropyl alcohol (IPA) were obtained from Sigma-Aldrich and used as received.

3.2. Preparation of Substrates. Glass slides were cut into squares (2.5 cm × 2.5 cm) with a diamond-tipped scribe. They were then subsequently cleaned with Alconox solution (2 mg mL^{-1}), deionized water, acetone, and then isopropyl alcohol (IPA) in an ultrasonic bath for 10 min each and then rinsed and dried with compressed air. Next, the glass was plasma treated at ∼30 W for 3 min at a base pressure of 200 mTorr ambient air to remove residual organic material and activate the surface. The slides were then placed in a vacuum desiccator with a glass vial containing ∼100 μL of FOTS and put under house vacuum for a minimum of 3 h to passivate the surface. The surface was then rinsed thoroughly with IPA to remove any excess FOTS and leave only a monolayer behind. The contact angle of water with the resulting surface was 109°.

3.3. Preparation of Films. To compare the yield points of P3ATs based on alkyl side-chain length, solutions of P3PT, P3HT, P3HpT, P3OT, and P3DDT in chloroform (15 mg mL^{-1}) were prepared and allowed to stir overnight. The solutions of P3PT were heated to 50 °C for 10 min to promote dissolution before use. All solutions were then filtered with 1 μm glass microfiber (GMF) filter immediately before being spin-coated onto FOTS passivated glass using a Headway Research PWM32. We chose to spin-coat the films onto FOTS glass and transfer to PDMS. Spinning directly onto PDMS would require treatment with either oxygen plasma or UV-Ozone, which would embrittle the substrate. The solutions were spun at 500 rpm (250 rpm s^{-1} ramp) for 120 s, followed by 2000 rpm (1000 rpm s^{-1} ramp) for 30 s, which produced films 200–300 nm thick.

To examine the effect of film thickness on the yield point, solutions with various concentrations of P3DDT in chloroform (7.5–15.0 mg mL^{-1}) were made and allowed to stir overnight. These solutions were filtered and spin-coated as specified above, resulting in film thicknesses of 130–250 nm. Films of P3DDT for analysis by UV–vis were spin-coated onto the FOTS passivated glass slides at a spin speed of 500 rpm (250 rpm s^{-1} ramp) for 120 s followed by 2000 rpm (1000 rpm s^{-1} ramp) for 30 s. All films were dried under vacuum for 15 min to remove residual solvent.

3.4. Laser Detection of Yield Point (LADYP). PDMS was prepared as stated above and cut into rectangular strips (l = 8 cm, w = 1 cm, h = 0.4 cm). The polymer films were then transferred to the PDMS strips. Transferring the conjugated polymer films to the prestrained PDMS substrate was performed by initially scoring the films along the edges with a razor and placing the films against the PDMS. After applying a minimum amount of pressure to create a conformal seal between the PDMS and the conjugated polymer film, the glass/PDMS was separated from the glass/conjugated polymer film in one fast motion.[43] Micrographs were taken of the films at 0% strain to ensure clean transfer to the PDMS (e.g., no delamination, no cracking). The films were then strained using a computer-controlled stage, which applied strains to samples using a linear actuator. The samples were cyclically strained and relaxed, again increasing the strain with each cycle (i.e., 0% → 1% → 0% → 2% → 0% → 3% → 0%, etc.). At each point of relaxation, the sample was irradiated with a 5 mW, 532 nm laser beam; the laser beam was transmitted through the film onto a screen that was observed to detect diffraction. At the onset of diffraction, the strain was recorded, and micrographs were taken to look for visible buckles. After the onset of diffraction, micrographs were taken at each subsequent strain. When buckles were visible in the microscope, this strain was recorded, as was the strain where the diffraction peaks were persistent (i.e., lasted longer than 1 min).

3.5. UV–vis Spectroscopy and Analysis. The absorbance of the materials was measured using an Agilent 8453 UV–vis spectrophotometer. The wavelength range measured was 850–300 nm with a step size of 1 nm. The films were transferred to PDMS as stated above. Absorption spectra of the films on PDMS were initially taken at 0% strain. The films were then strained to 10, 15, and 20% and clipped onto FOTS passivated glass at each strain before their absorption was measured.

The extent of order, as determined by UV–vis spectroscopy, has been correlated to increased tensile moduli in P3AT films. Spano et al. and others have shown that aggregates of P3HT in solid films can be considered as weakly interacting H aggregates, due to cofacial π–π stacking and weak excitonic coupling.[32,44−47] We used this model to compare trends in aggregation and aggregate order from the UV–vis absorption spectra of the polymer thin films, in an attempt to correlate these values with the yield point.

In the aggregated state (i.e., crystallites and other aggregates in solid films), coupled electron-vibrational (vibronic) transitions determine the absorption of weakly interacting H aggregates and can be modeled as Gaussian fits by

DOI: 10.1021/acsami.5b08628
ACS Appl. Mater. Interfaces 2015, 7, 23257−23264

$$A(E) \propto \sum_{m=0}\left(\frac{S^m}{m!}\right) \times \left(1 - \frac{We^{-S}}{2E_p}\sum_{n\neq m}\frac{S^n}{n!(n-m)}\right)^2 \times \exp\left(\frac{-\left(E - E_{00} - mE_p - \frac{1}{2}WS^m e^{-S}\right)^2}{2\sigma^2}\right)$$

In the above equation, A is the absorption by an aggregate as a function of the photon energy (E). E_{00} is the energy of the 0 → 0 vibronic transition, which is allowed assuming some disorder in the aggregates. S is the Huang–Rhys factor, which quantifies the nuclear potential well shift upon vibronic transition from the ground state to the excited state. It is calculated from absorption and emission spectra, and is set to 1 for P3ATs.[45] E_p is the intermolecular vibration energy, which (in the case where $S = 1$) is the difference in energy between the vibrational levels in the excited state. It is set to 0.179 eV as determined by Raman spectroscopy. W is the free exciton bandwidth, which is related to the nearest neighbor interchain excitonic coupling. Upon coupling, a dispersion of the energies occurs, the width of which is equal to W (which is four times the nearest neighbor coupling). W is also inversely related to conjugation length; a lower W indicates better ordering of the aggregates. The terms m and n are the ground- and excited state vibrational levels and σ is the Gaussian line width.

The parameters E_{00}, W, σ, and a scaling factor were found by using Matlab to perform a least-squares fit to the experimental absorption data in the region of 1.93 to 2.25 eV. This region was selected because the absorption is dominated by the polymer aggregates. Above 2.30 eV, the amorphous polymer dominates absorption.[48]

4. RESULTS AND DISCUSSION

We began by exploring the effect of side-chain length on the yield point of P3ATs (Figure 3). P3PT (n = 5), P3HT (n = 6), P3HpT (n = 7), P3OT (n = 8), and P3DDT (n = 12) were selected because they cover a wide range of side-chain lengths. P3AT films of similar thicknesses (~200–300 nm) were prepared to isolate the effect of the side-chain length. To confirm that the diffraction was correlated with the appearance of buckles in the thin films, we tracked three separate parameters: the strain at which diffraction of the laser first occurred, the strain at which diffraction lasted longer than 1 min, and the strain at which buckles were visible in the optical microscope. Table 1 summarizes the LADYP data of the P3ATs. A correlation between increasing strain and increasing alkyl side-chain length was observed for all three parameters.

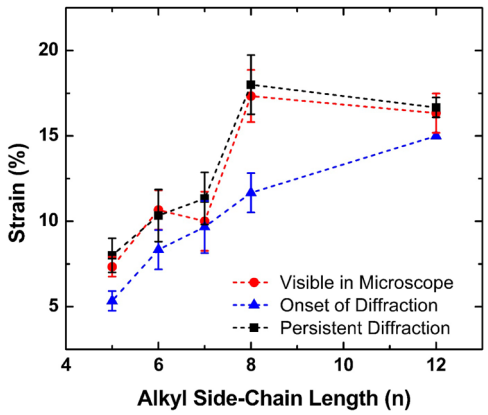

Figure 3. Yield point vs alkyl side-chain length for the P3ATs. All films were transferred to an elastic PDMS substrate and subsequently strained until the yield point, as determined by the appearance of buckles, was observed.

Table 1. Summary of the Yield Point vs Alkyl Side-Chain Length for the P3ATs As Measured in FOE Systems[a]

polymer	buckles in microscope strain (%)	onset of diffraction strain (%)	persistent diffraction strain (%)
P3PT	7.3 ± 0.6	5.3 ± 0.6	8.0 ± 1.0
P3HT	10.6 ± 1.2	8.3 ± 1.2	10.3 ± 1.5
P3HpT	10.0 ± 1.7	9.7 ± 1.5	11.3 ± 1.5
P3OT	17.3 ± 1.5	11.7 ± 1.2	18.0 ± 1.7
P3DDT	16.3 ± 1.2	15.0 ± 0.0	16.7 ± 0.6

[a]The persistent diffraction agrees well with the visibility of buckles in the microscope.

This trend agrees with previously reported results of a dependence on the side-chain length of other mechanical properties (i.e., compliance and ductility) in P3ATs.[11,12] We also found that the initial diffraction peaks lasted less than 1 min and occurred at lower strains than the visibility of buckles in the microscope. This observation suggested the onset of diffraction was not attributable to the yield point, but instead to the viscoelasticity of the PDMS.[43] There was a very strong agreement between the strains at which buckles were visible by microscope and the strains at which the LADYP diffraction peaks lasted longer than 1 min. When the diffraction lasted longer than 1 min, the buckles were in a more permanent state, meaning the film has been plastically deformed and the yield point had been passed. The increase in yield point for the P3ATs from n = 5 (P3PT) to n = 8 (P3OT) is attributed to the decreasing glass transition temperature with alkyl side-chain length, which results in greater chain mobility.[12,49] The observation that yield point decreases from n = 8 (P3OT) to n = 12 (P3DDT), even though the glass transition temperatures of P3OT and P3DDT are similar, is parallel to our earlier observation that crack-onset strain decreases over this same interval.[11] For P3ATs, surface energy decreases with increasing length of the alkyl chain, and reduced adhesion for polymers with longer side chains localizes strain to thin areas and defects in regions of local delamination.[11] Cracks thus form sooner in poorly adhered films than in perfectly adhered films, in which strain in the film is equal to the strain in the substrate at every point.[11,40] The same effect might produce earlier plastic deformation in P3DDT than in P3OT, though we cannot rule out the possibility that P3ATs with long side chains (n > 8) actually have a shorter elastic regime intrinsically. Micrographs of representative films just below (left column) and above (right column) the yield point are in Figure 4. In the micrographs of the films strained below the yield point, no sign of film buckling is observed. However, when the yield point is reached, the film is deformed and upon relaxation forms buckles out-of-plane, perpendicular to the direction of strain.

The effect of film thickness on the yield point of one of the P3ATs, P3DDT was also assessed using LADYP. The strain (in percent) is plotted against the film thickness in Figure 5. The yield point was stable above a thickness of 156 ± 10 nm to at least 251 ± 26 nm (17.7 ± 3.2% and 17.0 ± 1.0%, respectively, for the yield point determined by laser diffraction peaks lasting longer than 1 min); however, below this thickness, there was a substantial increase in the yield point strain. At a thickness of 147 ± 6 nm, the yield point increased slightly to 19.7 ± 0.6%.

When the film thickness was further decreased to 129 ± 5 nm, a much more substantial increase in yield point was observed (40.7 ± 3.2%). The observation of a large increase in the yield point strain with decreasing thickness agrees with

DOI: 10.1021/acsami.5b08628
ACS Appl. Mater. Interfaces 2015, 7, 23257–23264

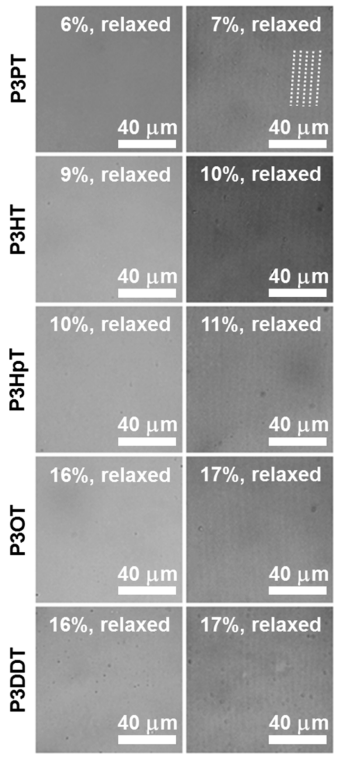

Figure 4. Micrographs of representative films of the P3ATs studied in this work. The micrographs in the column on the left are of films in the relaxed state which had been strained just below the yield point. The micrographs in the column on the right are of films in the relaxed state after they have been strained above the yield point. The dashed lines drawn in the P3PT micrograph in the right column are eye guides to highlight buckling of the film.

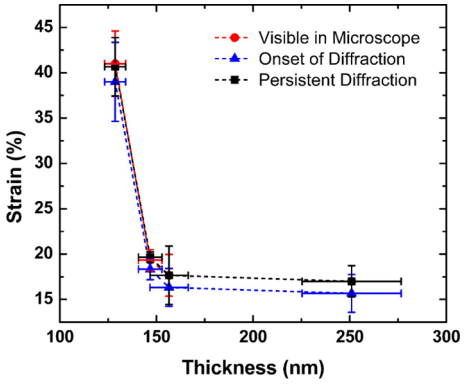

Figure 5. Yield point vs thickness for P3DDT. All films were prepared and evaluated as described above.

similar measurements of polystyrene.[17] These results suggest that in addition to alkyl side-chain length, the film thickness is a parameter that can, at least below the critical film thickness, be adjusted to tune film elasticity.[10,31,50]

To understand the evolution of the microstructure of the polymer around the yield point, we evaluated thin films of P3DDT under strain with the weakly interacting H-aggregate model developed by Spano and used by others.[12,44,45,47,51] We recorded the polarized absorption (both parallel and perpendicular to the direction of strain) of films of P3DDT unstrained, and at strains below, near, and above the yield point (10, 15, and 20%). The spectra were then evaluated with a MATLAB program that performed a least-squares fit of the weakly interacting H-aggregate model to the data. To isolate the effects of the strain and eliminate any film-to-film variations, the calculated parameters were then normalized to the unstrained values (Figure 6). We found that the quantity of

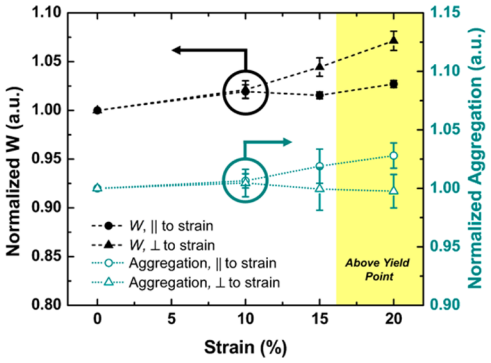

Figure 6. Evolution of weakly interacting H-aggregate model parameters with strain in P3DDT. The measurements were taken with polarized light both parallel and perpendicular to the direction of strain. *W* is the exciton bandwidth and is inversely related to conjugation length. The region above the yield point as determined by buckling onset is highlighted in yellow.

aggregates both perpendicular and parallel to the strain was essentially equal to each other up to about 10% strain. Above 10% strain, the quantity of aggregates perpendicular to the strain decreased as aggregates were pulled apart, while the quantity of aggregates parallel to the strain increased as chains were aligned and aggregated along the strained axis. Likewise, the aggregate quality, as indicated by the exciton bandwidth, *W*, the inverse of which is related to conjugation length of the polymer, both perpendicular and parallel to the strain were equivalent at 0% and 10% strain. Above 10% strain, the *W* value increased considerably perpendicular to strain. The *W* value parallel to strain decreased from 10% to 15% strain, suggesting an improvement in the ordering of the aggregates, before it increased from 15% to 20% strain. One possible explanation for this observation is that chains have begun slipping past each other to a less favorable configuration,[52] which agrees with our findings that the yield point of P3DDT is above 15% but below 20% strain.

Finally, we utilized the yield point found by LADYP, the crack-onset determined by the same cyclic straining, and the tensile modulus previously reported by us for the P3ATs[11,12] to approximate (very roughly) their stress–strain curves (Figure 7), so that it would be possible to calculate the modulus of resilience and estimate the modulus of toughness. We made the assumption that the stress–strain curve can be approximated by the tensile modulus (i.e., a straight line) to the yield point and that above the yield point, the stress remains unchanged until crack-onset, which we consider the strain at fracture (though we point out that it is not yet possible to know the stress at fracture from FOE systems, and this uncertainty is why one can only estimate the total energy absorbed at this point, i.e., the toughness, very roughly). This highly simplified curve shape (i.e., the behavior from the yield point to the strain at fracture is approximated by a horizontal line) is nevertheless similar to the stress-strain curve previously reported for bulk P3HT.[36,53] We then used the curves to determine the moduli of resilience and to roughly estimate the modulus of toughness for the P3ATs. In the cases of P3PT and P3HT, the crack-onset strain was

DOI: 10.1021/acsami.5b08628
ACS Appl. Mater. Interfaces 2015, 7, 23257–23264

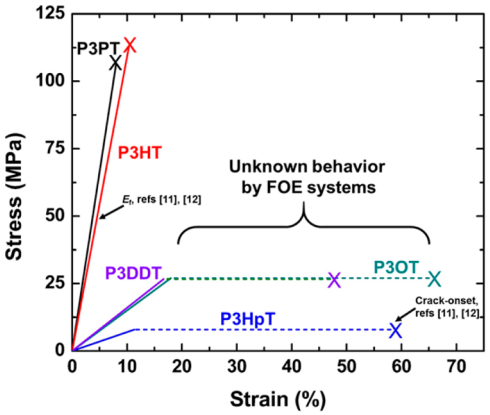

Figure 7. Approximated stress−strain curves for the P3ATs based on this work and that of refs 11 and 12.

lower than the yield point strain, however, we attributed this to differences in the preparation of the substrates and inhomogeneities in thickness in the films (which localize strain and produce cracks).[11,12]

Because the goal of these calculations was to estimate roughly the resilience and toughness, we estimated the crack-onset to be equal to the yield point in these cases. The mechanical properties derived from a typical stress−strain curve are summarized in Table 2. We found that although the higher modulus materials (i.e., P3PT and P3HT) have a higher approximate modulus of resilience, the P3OT and P3DDT films had a much higher modulus of toughness due to their greater crack-onset strain. This approximation suggests that, at least in the technologically relevant FOE systems, the films of P3OT and P3DDT can absorb a greater amount of energy before film failure due to cracking. The toughness of these films is important particularly in outdoor or wearable applications, where the resistance to fracture due to sudden unintended impact events (e.g., an object being accidentally dropped onto the device) is critical for continued real world device performance.

5. CONCLUSION

We described a new technique for measuring the yield point of polymer thin films supported on elastic substrates, LADYP, which provided insights on the effects of alkyl side-chain length and film thickness on this previously difficult to measure mechanical property. Experimental results indicated a correlation between alkyl side-chain length with yield point and a critical film thickness below which the yield point increases by up to a factor of 3. These findings were then used to roughly estimate the modulus of resilience and modulus of toughness of FOE systems to inform the design of more robust materials and devices for portable, outdoor, and wearable applications. Further investigation of the effects of the amount of crystallinity or aggregation of the thin films, adhesion of the film to the substrate, rate-dependency of strain on the yield point, and substrate mechanical properties (e.g., tensile modulus and elastic limit) will be necessary to understand fully how devices will perform under real world stresses. Moreover, the method we described is highly practical, as the onset of buckling may not represent the yield point one would obtain in a typical tensile test. Deviations could arise from the highly anisotropic geometry of a thin film, microstructures that depend on depth, the adhesion with the substrate, and unequal chemical environments at the top and bottom surfaces of the film. Nevertheless, it is the properties of the film when integrated with a flexible or stretchable substrate, not those of a bulk sample, that will determine the extent to which a real device can be deformed.

AUTHOR INFORMATION

Corresponding Author

*D. J. Lipomi. E-mail: dlipomi@ucsd.edu.

Notes

The authors declare no competing financial interest.

ACKNOWLEDGMENTS

This work was supported by the Air Force Office of Scientific Research (AFOSR) Young Investigator Program, grant number FA9550-13-1-0156. Additional support was provided by the National Science Foundation Graduate Research Fellowship, awarded to both S. Savagatrup and A.V. Zaretski, the UC LEADS fellowship and the STARS Summer Research Program, awarded to A. S.-C. Chiang, and by laboratory startup funds from the University of California, San Diego. The authors thank Prof. Frank Spano for helpful discussions.

REFERENCES

(1) Lipomi, D. J.; Bao, Z. Stretchable, Elastic Materials and Devices for Solar Energy Conversion. *Energy Environ. Sci.* **2011**, *4*, 3314−3328.
(2) Bruner, C.; Miller, N. C.; McGehee, M. D.; Dauskardt, R. H. Molecular Intercalation and Cohesion of Organic Bulk Heterojunction Photovoltaic Devices. *Adv. Funct. Mater.* **2013**, *23*, 2863−2871.
(3) Krebs, F. C.; Nielsen, T. D.; Fyenbo, J.; Wadstrøm, M.; Pedersen, M. S. Manufacture, Integration and Demonstration of Polymer Solar Cells in a Lamp for the "Lighting Africa" Initiative. *Energy Environ. Sci.* **2010**, *3*, 512−525.

Table 2. Summary of the Mechanical Properties of the P3ATs As Measured in FOE Systems[a]

polymer	tensile modulus (GPa)	yield point strain (%)	crack-onset strain (%)	approximate modulus of resilience (MPa)	approximate modulus of toughness (MPa)
P3PT	1.33 ± 0.14[12]	8.0 ± 1.0	6.3 ± 0.6	4.3 ± 0.9	4.3 ± 0.9
P3HT	1.09 ± 0.15[11]	10.3 ± 1.5	9.0 ± 1.2[11]	5.8 ± 1.5	5.8 ± 1.5
P3HpT	0.07 ± 0.01[12]	11.3 ± 1.5	58.0 ± 2.0[12]	0.4 ± 0.1	4.2 ± 0.8
P3OT	0.15 ± 0.05[11]	18.0 ± 1.7	65.0 ± 2.5[11]	2.4 ± 0.9	15.1 ± 4.6
P3DDT	0.16 ± 0.07[11]	16.7 ± 0.6	47.0 ± 3.1[11]	2.2 ± 1.0	10.3 ± 3.8

[a]Crack-onset and modulus measurements were performed with elastomer substrates cured at room temperature between 36 and 48 h, whereas the yield point measurements were performed on substrates cured at 70 °C for 25 min. The error for the moduli of resilience and toughness were calculated as a propagation of error from the tensile modulus, yield point strain, and crack-onset strain measurements; the error does not include any contribution from the approximation of the curve shape.

DOI: 10.1021/acsami.5b08628
ACS Appl. Mater. Interfaces 2015, 7, 23257−23264

(4) O'Connor, T. F.; Rajan, K. M.; Printz, A. D.; Lipomi, D. J. Toward Organic Electronics with Properties Inspired by Biological Tissue. *J. Mater. Chem. B* **2015**, *3*, 4947−4952.
(5) Ghezzi, D.; Antognazza, M. R.; Maccarone, R.; Bellani, S.; Lanzarini, E.; Martino, N.; Mete, M.; Pertile, G.; Bisti, S.; Lanzani, G.; Benfenati, F. A Polymer Optoelectronic Interface Restores Light Sensitivity in Blind Rat Retinas. *Nat. Photonics* **2013**, *7*, 400−406.
(6) Seyedin, M. Z.; Razal, J. M.; Innis, P. C.; Wallace, G. G. Strain-Responsive Polyurethane/PEDOT:PSS Elastomeric Composite Fibers with High Electrical Conductivity. *Adv. Funct. Mater.* **2014**, *24*, 2957−2966.
(7) Savagatrup, S.; Printz, A. D.; O'Connor, T. F.; Zaretski, A. V.; Rodriquez, D.; Sawyer, E. J.; Rajan, K. M.; Acosta, R. I.; Root, S. E.; Lipomi, D. J. Mechanical Degradation and Stability of Organic Solar Cells: Molecular and Microstructural Determinants. *Energy Environ. Sci.* **2015**, *8*, 55−80.
(8) Savagatrup, S.; Printz, A. D.; O'Connor, T. F.; Zaretski, A. V.; Lipomi, D. J. Molecularly Stretchable Electronics. *Chem. Mater.* **2014**, *26*, 3028−3041.
(9) Stafford, C. M.; Harrison, C.; Beers, K. L.; Karim, A.; Amis, E. J.; VanLandingham, M. R.; Kim, H.-C.; Volksen, W.; Miller, R. D.; Simonyi, E. E. A Buckling-Based Metrology for Measuring the Elastic Moduli of Polymeric Thin Films. *Nat. Mater.* **2004**, *3*, 545−550.
(10) Stafford, C. M.; Guo, S.; Harrison, C.; Chiang, M. Y. M. Combinatorial and High-Throughput Measurements of the Modulus of Thin Polymer Films. *Rev. Sci. Instrum.* **2005**, *76*, 062207.
(11) Savagatrup, S.; Makaram, A. S.; Burke, D. J.; Lipomi, D. J. Mechanical Properties of Conjugated Polymers and Polymer-Fullerene Composites as a Function of Molecular Structure. *Adv. Funct. Mater.* **2014**, *24*, 1169−1181.
(12) Savagatrup, S.; Printz, A. D.; Rodriquez, D.; Lipomi, D. J. Best of Both Worlds: Conjugated Polymers Exhibiting Good Photovoltaic Behavior and High Tensile Elasticity. *Macromolecules* **2014**, *47*, 1981−1992.
(13) Keddie, J. L.; Jones, R. L.; Cory, R. A. Size-Dependent Depression of the Glass Transition Temperature in Polymer Films. *Europhys. Lett.* **1994**, *27*, 59−64.
(14) Ellison, C. J.; Torkelson, J. M. The Distribution of Glass-Transition Temperatures in Nanoscopically Confined Glass Formers. *Nat. Mater.* **2003**, *2*, 695−700.
(15) Fakhraai, Z.; Forrest, J. A. Measuring the Surface Dynamics of Glassy Polymers. *Science* **2008**, *319*, 600−604.
(16) O'Connell, P. A.; McKenna, G. B. Rheological Measurements of the Thermoviscoelastic Response of Ultrathin Polymer Films. *Science* **2005**, *307*, 1760−1763.
(17) Gurmessa, B. J.; Croll, A. B. Onset of Plasticity in Thin Polystyrene Films. *Phys. Rev. Lett.* **2013**, *110*, 074301.
(18) Gurmessa, B.; Croll, A. B. Influence of Thin Film Confinement on Surface Plasticity in Polystyrene and Poly(2-Vinylpyridine) Homopolymer and Block Copolymer Films. *Macromolecules* **2015**, *48*, 5670−5676.
(19) Jørgensen, M.; Norrman, K.; Krebs, F. C. Stability/Degradation of Polymer Solar Cells. *Sol. Energy Mater. Sol. Cells* **2008**, *92*, 686−714.
(20) Jørgensen, M.; Norrman, K.; Gevorgyan, S. A.; Tromholt, T.; Andreasen, B.; Krebs, F. C. Stability of Polymer Solar Cells. *Adv. Mater.* **2012**, *24*, 580−612.
(21) Trznadel, M.; Pron, A.; Zagorska, M.; Chrzaszcz, R.; Pielichowski, J. Effect of Molecular Weight on Spectroscopic and Spectroelectrochemical Properties of Regioregular Poly(3-Hexylthiophene). *Macromolecules* **1998**, *31*, 5051−5058.
(22) Babel, A.; Jenekhe, S. A. Field-Effect Mobility of Charge Carriers in Blends of Regioregular Poly(3-Alkylthiophene)s. *J. Phys. Chem. B* **2003**, *107*, 1749−1754.
(23) Babel, A.; Jenekhe, S. A. Alkyl Chain Length Dependence of the Field-Effect Carrier Mobility in Regioregular Poly(3-Alkylthiophene)s. *Synth. Met.* **2005**, *148*, 169−173.
(24) Brinkmann, M. Structure and Morphology Control in Thin Films of Regioregular Poly(3-Hexylthiophene). *J. Polym. Sci., Part B: Polym. Phys.* **2011**, *49*, 1218−1233.
(25) Ro, H. W.; Akgun, B.; O'Connor, B. T.; Hammond, M.; Kline, R. J.; Snyder, C. R.; Satija, S. K.; Ayzner, A. L.; Toney, M. F.; Soles, C. L.; DeLongchamp, D. M. Poly(3-Hexylthiophene) and [6,6]-Phenyl -C61-Butyric Acid Methyl Ester Mixing in Organic Solar Cells. *Macromolecules* **2012**, *45*, 6587−6599.
(26) Wang, C.; Rivnay, J.; Himmelberger, S.; Vakhshouri, K.; Toney, M. F.; Gomez, E. D.; Salleo, A. Ultrathin Body Poly(3-Hexylthiophene) Transistors with Improved Short-Channel Performance. *ACS Appl. Mater. Interfaces* **2013**, *5*, 2342−2346.
(27) Gargi, D.; Kline, R. J.; DeLongchamp, D. M.; Fischer, D. A.; Toney, M. F.; O'Connor, B. T. Charge Transport in Highly Face-On Poly(3-Hexylthiophene) Films. *J. Phys. Chem. C* **2013**, *117*, 17421−17428.
(28) Printz, A. D.; Savagatrup, S.; Rodriquez, D.; Lipomi, D. J. Role of Molecular Mixing on the Stiffness of Polymer:Fullerene Bulk Heterojunction Films. *Sol. Energy Mater. Sol. Cells* **2015**, *134*, 64−72.
(29) Dauskardt, R. H.; Lane, M.; Ma, Q.; Krishna, N. Adhesion and Debonding of Multi-Layer Thin Film Structures. *Eng. Fract. Mech.* **1998**, *61*, 141−162.
(30) Dupont, S. R.; Novoa, F.; Voroshazi, E.; Dauskardt, R. H. Decohesion Kinetics of PEDOT:PSS Conducting Polymer Films. *Adv. Funct. Mater.* **2014**, *24*, 1325−1332.
(31) Lee, J.-H.; Chung, J. Y.; Stafford, C. M. Effect of Confinement on Stiffness and Fracture of Thin Amorphous Polymer Films. *ACS Macro Lett.* **2012**, *1*, 122−126.
(32) Awartani, O.; Lemanski, B. I.; Ro, H. W.; Richter, L. J.; DeLongchamp, D. M.; O'Connor, B. T. Correlating Stiffness, Ductility, and Morphology of Polymer:Fullerene Films for Solar Cell Applications. *Adv. Energy Mater.* **2013**, *3*, 399−406.
(33) Savagatrup, S.; Chan, E.; Renteria-Garcia, S. M.; Printz, A. D.; Zaretski, A. V.; O'Connor, T. F.; Rodriquez, D.; Valle, E.; Lipomi, D. J. Plasticization of PEDOT:PSS by Common Additives for Mechanically Robust Organic Solar Cells and Wearable Sensors. *Adv. Funct. Mater.* **2015**, *25*, 427−436.
(34) Printz, A. D.; Savagatrup, S.; Burke, D. J.; Purdy, T. N.; Lipomi, D. J. Increased Elasticity of a Low-Bandgap Conjugated Copolymer by Random Segmentation for Mechanically Robust Solar Cells. *RSC Adv.* **2014**, *4*, 13635−13643.
(35) Kim, H. J.; Kim, J.; Ryu, J.; Kim, Y.; Kang, H.; Lee, W. B.; Kim, T.; Kim, B. J. Architectural Engineering of Rod−Coil Compatibilizers for Producing Mechanically and Thermally Stable Polymer Solar Cells. *ACS Nano* **2014**, *8*, 10461−10470.
(36) Kim, J.-S.; Kim, J.-H.; Lee, W.; Yu, H.; Kim, H. J.; Song, I.; Shin, M.; Oh, J. H.; Jeong, U.; Kim, T.-S.; Kim, B. J. Tuning Mechanical and Optoelectrical Properties of Poly(3-Hexylthiophene) through Systematic Regioregularity Control. *Macromolecules* **2015**, *48*, 4339−4346.
(37) Torres, J. M.; Stafford, C. M.; Vogt, B. D. Impact of Molecular Mass on the Elastic Modulus of Thin Polystyrene Films. *Polymer* **2010**, *51*, 4211−4217.
(38) O'Connor, B.; Chan, E. P.; Chan, C.; Conrad, B. R.; Richter, L. J.; Kline, R. J.; Heeney, M.; McCulloch, I.; Soles, C. L.; DeLongchamp, D. M. Correlations between Mechanical and Electrical Properties of Polythiophenes. *ACS Nano* **2010**, *4*, 7538−7544.
(39) Lipomi, D. J.; Chong, H.; Vosgueritchian, M.; Mei, J.; Bao, Z. Toward Mechanically Robust and Intrinsically Stretchable Organic Solar Cells: Evolution of Photovoltaic Properties with Tensile Strain. *Sol. Energy Mater. Sol. Cells* **2012**, *107*, 355−365.
(40) Lu, N.; Wang, X.; Suo, Z.; Vlassak, J. Metal Films on Polymer Substrates Stretched beyond 50%. *Appl. Phys. Lett.* **2007**, *91*, 221909.
(41) Jeong, Y. R.; Park, H.; Jin, S. W.; Hong, S. Y.; Lee, S.-S.; Ha, J. S. Highly Stretchable and Sensitive Strain Sensors Using Fragmentized Graphene Foam. *Adv. Funct. Mater.* **2015**, *25*, 4228−4236.
(42) O'Connor, T. F.; Zaretski, A. V.; Shiravi, B. A.; Savagatrup, S.; Printz, A. D.; Diaz, M. I.; Lipomi, D. J. Stretching and Conformal Bonding of Organic Solar Cells to Hemispherical Surfaces. *Energy Environ. Sci.* **2014**, *7*, 370−378.
(43) Meitl, M. A.; Zhu, Z.-T.; Kumar, V.; Lee, K. J.; Feng, X.; Huang, Y. Y.; Adesida, I.; Nuzzo, R. G.; Rogers, J. A. Transfer Printing by

DOI: 10.1021/acsami.5b08628
ACS Appl. Mater. Interfaces 2015, 7, 23257−23264

Kinetic Control of Adhesion to an Elastomeric Stamp. *Nat. Mater.* **2006**, *5*, 33−38.
(44) Spano, F. C. Modeling Disorder in Polymer Aggregates: The Optical Spectroscopy of Regioregular Poly(3-Hexylthiophene) Thin Films. *J. Chem. Phys.* **2005**, *122*, 234701.
(45) Clark, J.; Chang, J.-F.; Spano, F. C.; Friend, R. H.; Silva, C. Determining Exciton Bandwidth and Film Microstructure in Polythiophene Films Using Linear Absorption Spectroscopy. *Appl. Phys. Lett.* **2009**, *94*, 163306.
(46) Spano, F. C.; Clark, J.; Silva, C.; Friend, R. H. Determining Exciton Coherence from the Photoluminescence Spectral Line Shape in poly(3-Hexylthiophene) Thin Films. *J. Chem. Phys.* **2009**, *130*, 074904.
(47) Turner, S. T.; Pingel, P.; Steyrleuthner, R.; Crossland, E. J. W.; Ludwigs, S.; Neher, D. Quantitative Analysis of Bulk Heterojunction Films Using Linear Absorption Spectroscopy and Solar Cell Performance. *Adv. Funct. Mater.* **2011**, *21*, 4640−4652.
(48) Pingel, P.; Zen, A.; Abellón, R. D.; Grozema, F. C.; Siebbeles, L. D. A.; Neher, D. Temperature-Resolved Local and Macroscopic Charge Carrier Transport in Thin P3HT Layers. *Adv. Funct. Mater.* **2010**, *20*, 2286−2295.
(49) Savagatrup, S.; Printz, A. D.; Wu, H.; Rajan, K. M.; Sawyer, E. J.; Zaretski, A. V.; Bettinger, C. J.; Lipomi, D. J. Viability of Stretchable Poly(3-Heptylthiophene) (P3HpT) for Organic Solar Cells and Field-Effect Transistors. *Synth. Met.* **2015**, *203*, 208−214.
(50) Stafford, C. M.; Vogt, B. D.; Harrison, C.; Julthongpiput, D.; Huang, R. Elastic Moduli of Ultrathin Amorphous Polymer Films. *Macromolecules* **2006**, *39*, 5095−5099.
(51) Savagatrup, S.; Rodriquez, D.; Printz, A. D.; Sieval, A. B.; Hummelen, J. C.; Lipomi, D. J. [70]PCBM and Incompletely Separated Grades of Methanofullerenes Produce Bulk Heterojunctions with Increased Robustness for Ultra-Flexible and Stretchable Electronics. *Chem. Mater.* **2015**, *27*, 3902−3911.
(52) Yamagata, H.; Pochas, C. M.; Spano, F. C. Designing J-and H-Aggregates through Wave Function Overlap Engineering: Applications to poly(3-Hexylthiophene). *J. Phys. Chem. B* **2012**, *116*, 14494−14503.
(53) Koch, F. P. V.; Rivnay, J.; Foster, S.; Müller, C.; Downing, J. M.; Buchaca-domingo, E.; Westacott, P.; Yu, L.; Yuan, M.; Baklar, M.; Fei, Z.; Luscombe, C.; McLachlan, M. A.; Heeney, M.; Rumbles, G.; Silva, C.; Salleo, A.; Nelson, J.; Smith, P.; Stingelin, N. The Impact of Molecular Weight on Microstructure and Charge Transport in Semicrystalline Polymer Semiconductors−Poly(3-Hexylthiophene), a Model Study. *Prog. Polym. Sci.* **2013**, *38*, 1978−1989.

DOI: 10.1021/acsami.5b08628
ACS Appl. Mater. Interfaces 2015, 7, 23257−23264